Ion−Molecule Chemistry of BF_3 in Clusters: Mass Spectrometric and ab Initio Computational Study of $B_nF_{3n-1}^+$

David A. Hales,* Pamela A. Haile, Michael P. Barker, and Heather L. Hunt

Department of Chemistry, Hendrix College, 1600 Washington Avenue, Conway, Arkansas 72032-3080

Received: July 30, 1998

Boron trifluoride clusters are formed in a supersonic expansion and ionized by electron impact. The resulting ion distribution is analyzed by time-of-flight mass spectrometry. The only consistently observed, extended series of peaks in EI of BF_3 clusters is $B_nF_{3n-1}^+$. Ab initio modeling of these ions informs our speculation regarding their internal structure and ion−molecule chemistry involved in their formation. Formation of $B_2F_5^{\delta+}$ is computationally predicted to occur in all of the cluster ions we observe ($n = 2-8$) except $B_3F_8^+$. $BF_4^{\delta-}$ units are evident in the predicted structure of $B_8F_{23}^+$.

1. Introduction

Boron and its compounds have proven interesting to the inorganic chemistry community for many years. The three-center, two-electron bonds in diborane and the polyhedral structures of higher boranes are now standard textbook material. While not as extensively studied as the boranes, compounds of boron and fluorine also have received some attention. Boron trifluoride, the simplest isolable boron fluoride, is a useful Lewis acid. Diboron tetrafluoride (B_2F_4) is a theoretically interesting molecule[1] which has also attracted significant experimental attention.[2] Some higher boron fluorides are known, though they have received limited attention in both theory[3] and experiment.[4−7]

Boron trifluoride is of wide utility in the semiconductor manufacturing field. The majority of applications involve plasma processing of surfaces, largely p-type doping of Si.[8,9] The ability of BF_3 to etch Si and SiO_2 has also been investigated under plasma conditions.[9,10] The mixture of ionic and neutral species in a plasma environment ensures that ion−molecule encounters will take place and raises the plausible picture of ion−molecule chemistry in the plasma.

Even so, the ion−molecule chemistry of BF_3 has received scant attention. A large body of work exists on electron impact ionization and photoionization of BF_3, but these works are concerned with the ionization and fragmentation of isolated BF_3 molecules.[11−13] Cationic boron fluorides containing more than one boron atom are rare in the literature, appearing only in mass spectrometric studies of B_2F_4,[13,14] B_3F_5,[4] B_8F_{12},[5] and some heavier but incompletely characterized compounds,[15] where parent ionization potentials and fragment appearance potentials were measured, and fragmentation patterns were used to discern parent molecular structure.

In this work we examine some ion−molecule chemistry of boron trifluoride by electron impact ionization of molecular clusters. Upon ionization of a molecular cluster, the nascent ion is in contact with neighboring neutral molecules in the cluster. Ion−molecule reactions are obviously possible in this situation and have been observed in many chemical systems with both electron impact ionization[16,17] and photoionization.[18] When electron impact is employed with above-threshold electron energy, "evaporation" of neutrals from the clusters can be expected to take place due to excess energy deposited in the cluster in the ionization process. Therefore, the observed mass distribution is the result of reactions in and fragmentation of the clusters. Relative stabilities of the product cluster ions are reflected, rather than the initial distribution of neutral clusters.[19] This makes mass spectrometry an effective probe of ion−molecule chemistry within ionized clusters.

2. Experimental Technique

2.1. Mass Spectrometer. The locally constructed, two-chamber time-of-flight mass spectrometer is depicted in Figure 1. The instrument employs a Wiley−McLaren ion acceleration scheme[20] with pulsed voltages. The highest voltage electrode is a plate, and the focusing voltage and ground electrodes have centers of 90% transmission nickel mesh. The electrodes are 5.08 cm square with 1.27 cm spacing and 3.18 cm diameter circular mesh areas for ion transmission. The high-voltage pulser (HV1000, Directed Energy Inc., Fort Collins, CO; 900 V) provides an acceleration voltage rise time of 18 ns (10−90%) measured at the acceleration electrodes. The pulser output is connected directly to the high-voltage electrode and to the second electrode through a simple voltage divider for space focusing. The acceleration pulse is typically of 5 μs duration.

The ions have a velocity component perpendicular to the direction of acceleration because of the supersonic expansion in which the neutral clusters are formed. To compensate, a coarse deflector is positioned immediately following the acceleration region. The ions pass through an einzel lens and a pair of fine control deflectors between 15.5 and 25.9 cm downstream from the acceleration region, and 58.2 cm after acceleration the ions enter the gridless reflectron (14 cm deep, 3.2 cm inner diameter, 22 rings plus rear plate). The reflectron axis is set at an angle of 2.5° to the incident ion beam axis, so the ions are reflected at 5° to their initial path.

After exiting the reflectron, the ions travel 23.0 cm to a dual microchannel plate detector with a 2.5 cm diameter active area. The detector is completely encased in stainless steel wire cloth except for the ion path, which is a 3.2 cm diameter "window" of 90% transmission Ni mesh. The shielding both reduces electromagnetic pickup of the acceleration voltage pulse by the signal-carrying circuitry and prevents the detector voltage (−2 kV) from deflecting the ions when they pass the detector assembly on their way to the reflectron. The detector is appropriately angled so that the ion incidence is normal to the

* Corresponding author. Electronic mail: halesda@hendrix.edu.

10.1021/jp983226l CCC: $15.00
Published on Web 10/02/1998

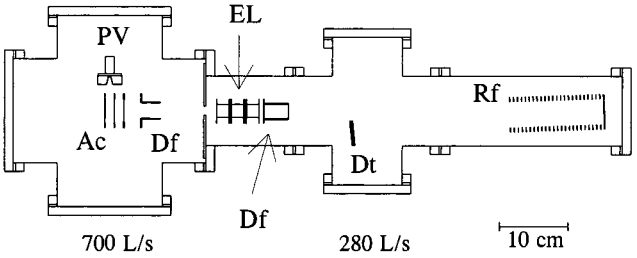

Figure 1. Time-of-flight mass spectrometer, top view. The electron beam for ionization is directed into the page and intersects with the cluster beam between the two leftmost acceleration electrodes. PV = pulsed valve with conical nozzle; Ac = acceleration electrodes; Df = deflectors; EL = einzel lens; Rf = reflectron; Dt = detector. Internal supports are omitted for clarity.

detector surface. The signal from the microchannel plates is first amplified (Comlinear CLC501) and then collected and averaged for 1000 sweeps with a digital summing oscilloscope (LeCroy 9310a, 400 MHz bandwidth, 100 MHz sampling rate). The averaged signal is transferred to a PC-compatible computer for analysis. The pulsed valve support system, detector mount, electron gun (see below), and all ion optics are constructed from commercially available components (eV parts, Kimball Physics Inc., Wilton Hill, NH). Each cycle of the experiment is initiated by a commercial pulsed valve driver (General Valve Iota One), and all subsequent timing is controlled with a Stanford Research Systems DG535 digital delay generator.

2.2. Electron Impact Ion Source. The electron gun used in this ion source is simple in design. The filament is enclosed in a cup-shaped repeller electrode, and the remaining face of the enclosure is an extractor electrode. Following the extractor are a focusing electrode and an exit orifice. The extractor and focusing electrode voltages are optimized with an eye toward both magnitude and resolution of the ion signal, while the repeller is fixed at an appropriate negative voltage and the exit is tied to the high-voltage ion acceleration electrode (grounded until the ion acceleration pulse). Clusters of BF_3 are formed by allowing a mixture of 5 mol % $^{11}BF_3$ in helium (Voltaix, North Branch, NJ) to expand into vacuum from a variable stagnation pressure of 1−7 bar. The expansion takes place through a pulsed molecular beam valve (General Valve series 9, 1.1 mm orifice) to which is attached a 1.27 cm long, 30° included angle, diverging conical nozzle. After a delay that allows the neutral clusters to drift to the acceleration region of the mass spectrometer, the electron beam is pulsed on by dropping the extractor electrode of the electron focusing optics from the repeller voltage to an appropriate focusing voltage. The electron beam pulse typically lasts 2−3 μs. The trigger for the ion acceleration voltage pulse is simultaneous with the end of the electron beam pulse.

3. Experimental Results

Electron impact ionization (100 eV) mass spectra of BF_3 clusters show the formation of several species, but one series of peaks dominates all others (Figure 2). This series of peaks is $B_nF_{3n-1}^+$, which we have observed for n = 1−8. The strongest member of the series, which is also the strongest peak in all our EI mass spectra, is BF_2^+ at m/e = 49. In these experiments, this species may be formed not only by EI of unclustered BF_3 molecules but also by EI of clusters followed by evaporation of neutral molecules until only BF_2^+ remains. The larger members of this series ($n \geq 2$) gradually decrease in intensity as n increases until the signal is too small to detect. There do not appear to be any "magic numbers" in this series to indicate special stability for certain structures.

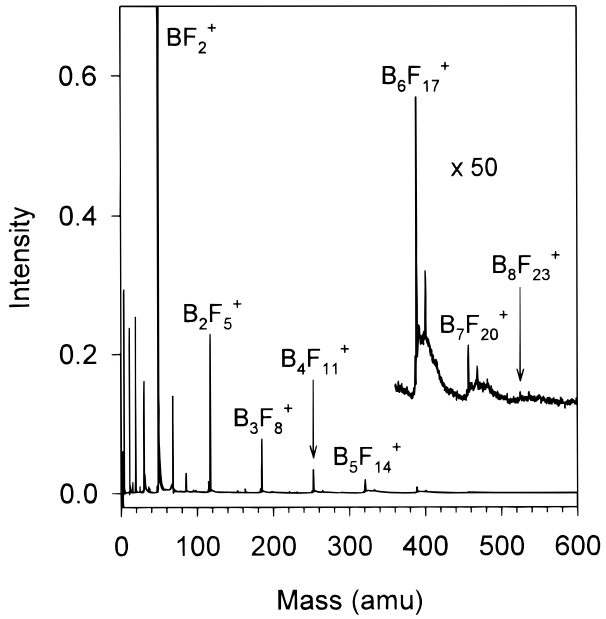

Figure 2. TOF mass spectrum of BF_3 clusters using 100 eV electron impact ionization and 6 bar stagnation pressure of 5% $^{11}BF_3$ in He.

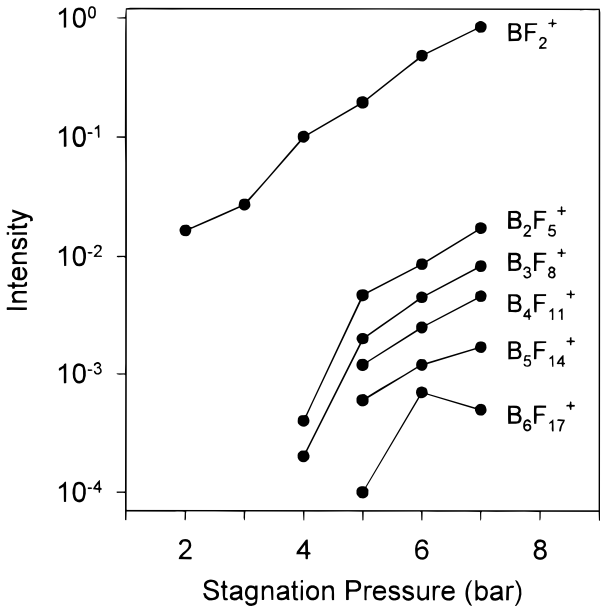

Figure 3. Dependence of $B_nF_{3n-1}^+$ signal on BF_3/He stagnation pressure.

Some of the other peaks observed in the EI spectra are easily identified as the normal products of electron impact on BF_3, e.g., BF_3^+, BF^+, B^+, and F^+. Close study reveals small peaks at m/e = 15 and 24.5, which are presumably BF^{2+} and BF_2^{2+}. These doubly charged species are most likely formed from single molecules (not clusters) of BF_3. Any small doubly charged clusters that are formed in the EI process could be expected to fragment rapidly into two singly charged fragments (a "coulomb explosion").[19,21] A peak is also seen at m/e = 85, which is most likely BF_3OH^+ formed from $BF_3{\cdot}H_2O$. Its presence is greatly reduced, but not eliminated, by inlet line bake-out and cryotrapping at −77 °C.

Figure 3 shows that, as expected, the intensity of larger clusters increases as the stagnation pressure of the gas mixture is increased.[22] The trends in Figure 3 indicate that still higher stagnation pressure would quite likely result in the formation

of even larger cluster ions, but at the present time our regulator limits us to 7 bar.

Variation of the electron energy results in no marked changes in the ion distribution. The ion signal simply decreases in a gradual fashion as the electron energy is decreased from 100 eV. It appears that the energy resolution available with our electron gun is insufficient to allow appearance potential measurements. The cause of the electron energy spread has not yet been determined. Though we are not able to measure the appearance potentials for these cluster ions, we can speculate about the values. The ionization energy of a molecule in a cluster is lower than the ionization energy of the isolated molecule due to solvation of the ion.[23] It is therefore likely that the appearance potentials for $B_nF_{3n-1}^+$ are all below 15.81 eV, the appearance potential for BF_2^+ from BF_3.[24]

4. Computational Modeling

Our understanding of the $B_nF_{3n-1}^+$ series is informed by simple molecular modeling. All calculations are performed using MacSpartan Plus (Wavefunction, Inc., Irvine, CA). Geometries of clusters with $n = 2-5$ are optimized by ab initio Hartree−Fock calculations with both 3-21G(*) and 6-31G* basis sets. Similar computational studies of larger structures in the series are also of significant interest, but optimization of these species with the 6-31G* basis set requires more powerful computational hardware than is presently available in our laboratory. Therefore, the $n = 6-8$ cluster ions are optimized at only the 3-21G(*) level.

The geometry optimizations begin with asymmetric structures and are carried out without symmetry constraints. Stepwise optimization of a structure by beginning with a low-level method, then using the result as the starting point for a higher level method, will generally result in significant time savings compared to optimization at a high computational level directly from the initial structure. With these $B_nF_{3n-1}^+$ clusters, a problem arises. Optimization at the semiempirical PM3 level frequently results in symmetric structures, and this symmetry is maintained when the PM3 structure is then used as the starting point for an ab initio [HF 3-21G(*) or 6-31G*] optimization. When vibrational frequencies are calculated for the optimized structures to ensure that they represent energy minima, it is found that the symmetric structures are indeed minima at the PM3 level, but not always at the ab initio levels. Therefore, the ab initio geometry optimizations must begin with asymmetric structures. These are generated either from scratch or by editing the result of a lower level optimization to break the symmetry. This process yields structures that are indeed energy minima, as indicated by a full complement of real vibrational frequencies, and are at least slightly asymmetric. Slightly broken symmetry appears to be required for energy minimization at our highest computational level.

Any species with the general formula $B_nF_{3n-1}^+$ has an even number of electrons, so a singlet ground state is possible. Full optimization of $B_2F_5^+$ with a triplet ground state results in an apparently dissociated molecule ($B_2F_4^+ + F$) that is 5.5 eV higher in energy than the optimized singlet state molecule. On the basis of this result, we assume singlet ground states for all the molecules in the $B_nF_{3n-1}^+$ series.

Structures obtained with both the 6-31G* and 3-21G(*) basis sets for $B_nF_{3n-1}^+$, $n = 2-5$, are shown schematically in Figure 4. The HF 6-31G* geometries are summarized numerically in Table 1 for $n = 2-4$, and the atomic charges are given in Table 2. The optimized structures can be broken down into approximately closed-shell fragments by inspection of bond lengths, atomic charges, and electron density isosurfaces. This model of the $B_nF_{3n-1}^+$ cluster ion as an aggregate of smaller parts is central to the discussion below.

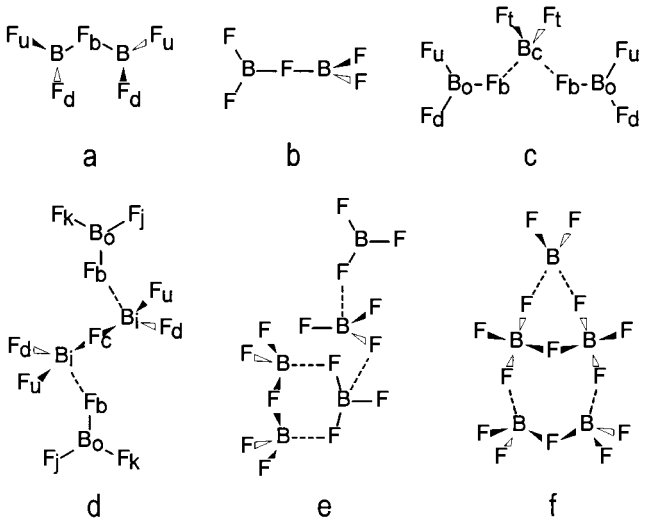

Figure 4. Schematic structures of $B_nF_{3n-1}^+$, $n = 2-5$: (a) $B_2F_5^+$, HF 6-31G*; (b) $B_2F_5^+$, HF 3-21G(*); (c) $B_3F_8^+$, HF 6-31G* and 3-21G(*); (d) $B_4F_{11}^+$, HF 6-31G* and 3-21G(*); (e) $B_5F_{14}^+$, HF 6-31G*; (f) $B_5F_{14}^+$, HF 3-21G(*). Subscripts are atomic labels referred to in the text and Tables 1 and 2. Dashed lines indicate weaker interactions between covalently bound fragments.

Thermodynamic data are presented in parts a and b of Table 3 for calculations using the 3-21G(*) and 6-31G* bases, respectively. Electronic energies in hartrees are the direct result of the ab initio calculations. The enthalpy of formation of each cluster ion is estimated by combining our computational results with experimentally determined values[25] of Δ_fH of gaseous BF_3 and BF_2^+, as shown in eq 1.

$$\Delta_fH_{298}(B_nF_{3n-1}^+) = E_{tot}(B_nF_{3n-1}^+) - [E_{tot}(BF_2^+) + (n-1)E_{tot}(BF_3)] + \Delta_fH(BF_2^+) + (n-1)\Delta_fH(BF_3) \quad (1)$$

The calculated total energy of $B_nF_{3n-1}^+$ is compared to the calculated total energy of $[BF_2^+ + (n-1)BF_3]$ to determine the change in energy due to formation of the cluster from this set of molecules. The experimental enthalpies of formation of $BF_2^+ + (n-1)BF_3$ are then added to this quantity to give an estimate for the enthalpy of formation of $B_nF_{3n-1}^+$. The experimental values are reported for 298 K, so in order for the derived enthalpies to pertain to 298 K, the total energies used in eq 1 include mean translational and internal energies calculated by standard statistical mechanical methods from the masses and theoretically predicted vibrational frequencies and rotational moments of inertia. The value used for $\Delta_fH(BF_2^+)$ conforms to the "ion convention" for treatment of the electron, so the $\Delta_fH_{298}(B_nF_{3n-1}^+)$ values are also "ion convention" values.[24] The final entry in Table 3a,b, ΔH(BF_3 loss), indicates the enthalpy change calculated from the Δ_fH values for the process $B_nF_{3n-1}^+ \rightarrow B_{n-1}F_{3n-4}^+ + BF_3$.

5. Discussion

5.1. $B_nF_{3n-1}^+$, $n = 1-5$. The $B_nF_{3n-1}^+$ series begins with BF_2^+, and this species dominates the mass spectrum. This is to be expected, since BF_2^+ is by far the most abundant ion formed in EI of BF_3 for electron energies above 18 eV.[11] The dominance of BF_2^+ in the EI mass spectrum is easily understood by recognizing that it is isoelectronic with BeF_2, which is a stable, linear molecule.[26] Geometry optimization at the 6-31G*

TABLE 1: Calculated Geometries (HF 6-31G*)

species	sym[a]	bond length (Å)[b]		bond angle (deg)[b]		dihedral angle (deg)[b,c]		
BF_3[d]	D_{3h}	B−F	1.301	F−B−F	120.00			
BF_2^+	$D_{\infty h}$	B−F	1.218	F−B−F	180.00			
$B_2F_5^+$	C_2	B−F_b	1.482	B−F_b−B	138.52	F_u−B−F_b−B	−157.01	−157.01
		B−F_u	1.255	F_b−B−F_u	112.25	F_d−B−F_b−B	23.32	23.29
		B−F_d	1.260	F_b−B−F_d	112.75			
				F_u−B−F_d	135.00			
$B_3F_8^+$	C_{2v}	B_c−F_t	1.280	F_t−B_c−F_t	129.38	F_b−B_c−F_b−B_o	−179.91	179.41
		B_c−F_b	1.621	F_b−B_c−F_b	92.65	F_u−B_o−F_b−B_c	0.18	0.09
		B_o−F_b	1.416	B_c−F_b−B_o	132.48	F_d−B_o−F_b−B_c	−179.81	179.91
		B_o−F_u	1.271	F_b−B_o−F_u	114.71			
		B_o−F_d	1.265	F_b−B_o−F_d	114.74			
				F_u−B_o−F_d	130.55			
$B_4F_{11}^+$	C_2	F_c−B_i	1.476	B_i−F_c−B_i	135.77	B_i−F_c−B_i−F_b	−76.03	−76.00
		B_i−F_b	2.147	F_c−B_i−F_u	112.12	B_i−F_c−B_i−F_u	−172.85	−172.82
		B_i−F_u	1.264	F_c−B_i−F_d	113.51	B_i−F_c−B_i−F_d	20.18	20.22
		B_i−F_d	1.268	F_c−B_i−F_b	87.33	F_c−B_i−F_b−B_o	−172.24	−172.21
		F_b−B_o	1.352	F_u−B_i−F_d	132.63	B_i−F_b−B_o−F_j	−2.68	−2.70
		B_o−F_j	1.285	F_u−B_i−F_b	97.32	B_i−F_b−B_o−F_k	177.43	177.41
		B_o−F_k	1.281	B_i−F_b−B_o	136.86			
				F_b−B_o−F_j	116.89			
				F_b−B_o−F_k	117.75			
				F_j−B_o−F_k	125.36			

[a] Exact for BF_3 and BF_2^+, approximate for others. [b] Subscripts refer to atomic labels in Figure 4. [c] This dual column indicates discernible difference between the two ends of the molecule; it is these small differences that make the point group assignments approximate. [d] Provided for comparison.

TABLE 2: Calculated Atomic Charges (HF 6-31G*)

species	atom[a]	charge	species	atom[a]	charge
$B_2F_5^+$	B	1.03	B_4F_{11}+	B_i	1.07
	F_b	−0.36		B_o	0.98
	F_u	−0.17		F_c	−0.38
	F_d	−0.19		F_u	−0.21
$B_3F_8^+$	B_c	1.10		F_d	−0.23
	B_o	1.02		F_b	−0.40
	F_t	−0.25		F_j	−0.25
	F_b	−0.39		F_k	−0.27
	F_u	−0.23			
	F_d	−0.20			

[a] Subscripts refer to atomic labels in Figure 4.

level predicts a $D_{\infty h}$ structure for BF_2^+, in agreement with this assessment. The formula $B_nF_{3n-1}^+$ can be broken down as $(BF_3)_{n-1}BF_2^+$, so it is logical to propose that larger members of the $B_nF_{3n-1}^+$ series are generated by production of a BF_2^+ ion, with expulsion of the F atom in the EI process, followed by rearrangement of the cluster around the BF_2^+ ion and evaporation of neutral BF_3 molecules.

It might be expected that the larger $B_nF_{3n-1}^+$ would look like $n-1$ BF_3 molecules surrounding a BF_2^+ ion. However, at the HF 6-31G* level, $B_2F_5^+$ is computationally predicted to have C_2 symmetry such that the optimized structure cannot be divided into distinct BF_2^+ and BF_3 fragments (Figures 4a and 5, Table 1). The bonds between the two boron atoms and the central fluorine atom are equivalent, and the charge is distributed in a symmetric fashion. The value for the electron density isosurface that is shown as a mesh framework in Figure 5 (also Figures 6 and 7) is 0.08 au. This value is chosen such that the isosurface should enclose the region between atoms if there is sufficient electron density to constitute a conventional covalent bond. (Note that these surfaces are significantly smaller than, and are not meant to represent, van der Waals contact surfaces.) The entire $B_2F_5^+$ ion is enclosed within a single surface, which we can interpret to mean that, electronically, it is a single molecular entity. The only major difference when this species is optimized at the 3-21G(*) level is that the ion has D_{2d} symmetry (Figure 4b); all conclusions about symmetric bonding are the same as for the C_2 cluster ion.

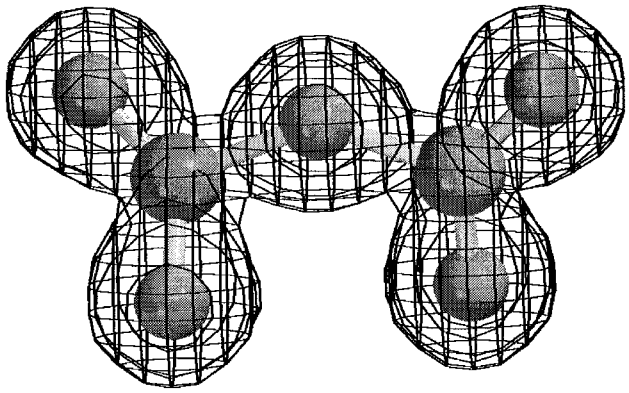

Figure 5. Structure of $B_2F_5^+$, optimized at the 6-31G* level. The larger spheres represent boron atoms, and the smaller spheres are fluorine atoms. The mesh framework is an electron density isosurface discussed in the text.

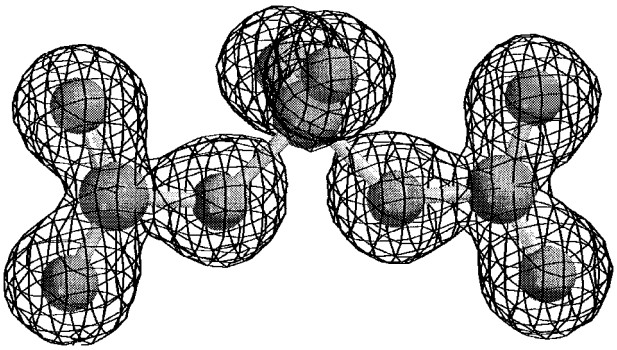

Figure 6. Structure of $B_3F_8^+$, optimized at the 6-31G* level. The larger spheres represent boron atoms, and the smaller spheres are fluorine atoms. The mesh framework is an electron density isosurface discussed in the text.

$B_3F_8^+$ optimizes to a structure with overall symmetry that is nearly C_{2v} at both 3-21G(*) and 6-31G* levels. The structure resulting from HF 6-31G* optimization is represented in Figures 4c and 6. If the symmetry were exact, all the atoms except the two labeled F_t in Figure 4c would be in a single plane. The isosurface in Figure 6 encloses three separate volumes that

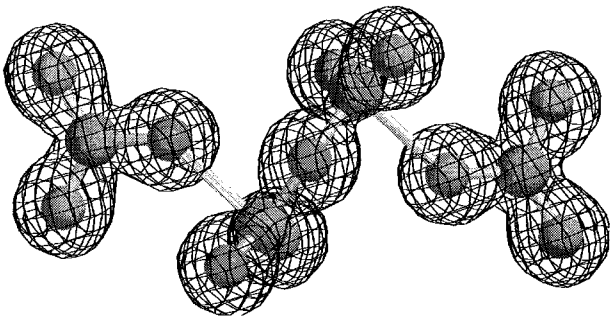

Figure 7. Structure of $B_4F_{11}^+$, optimized at the 6-31G* level. The C_2 axis is normal to the plane of the page. The mesh framework is an electron density isosurface discussed in the text. The separation into a B_2F_5 and two BF_3 units is readily apparent.

clearly resemble two BF_3 molecules coordinated through F atoms to the B atom in a bent BF_2 fragment. Each BF_3 fragment is planar, and the largest deviation of an atom in one BF_3 unit from the plane defined by the other BF_3 is only 0.034 Å. The B_c-F_b distance is fairly long at 1.621 Å, which is in line with a somewhat weakened interaction as compared to, for example, a B−F bond in BF_3 or the B−F_b distance in $B_2F_5^+$ (1.301 or 1.482 Å, respectively, Table 1). This structure is consonant with the idea of BF_3 molecules coordinated to a BF_2^+ ion, though the calculated atomic charges (Table 2) add to give $(BF_3^{0.20+})_2BF_2^{0.60+}$ and thus a less localized charge than the simple picture would indicate. The $B_3F_8^+$ structure has symmetry and distributed charge in common with the result for $B_2F_5^+$, but within this structure there is a uniquely identifiable $BF_2^{\delta+}$ fragment, which is absent from the $B_2F_5^+$ structure.

The optimized structure of $B_4F_{11}^+$ has approximate C_2 symmetry at both computational levels (Figures 4d and 7). The B_i-F_b bond distances (2.146 Å) are approximately 45% longer than bridging F−B distances (1.48 Å) and 70% longer than typical terminal F−B distances (1.26−1.28 Å) calculated here for $B_2F_5^+$ fragments. This, coupled with the low calculated electron density between each B_i-F_b pair as shown by the electron density isosurface, leads to the reasonable interpretation that $B_4F_{11}^+$ is best understood as two BF_3 molecules coordinated to an easily recognizable $B_2F_5^+$ unit. This view is supported by the calculated atomic charges, which add to $(BF_3^{0.06+})_2$-$B_2F_5^{0.88+}$.

Four units, essentially three BF_3 molecules and a $B_2F_5^+$ ion, comprise the C_1 structure predicted for $B_5F_{14}^+$ at the HF 6-31G* level (Figure 4e). The calculated atomic charges add to give $B_2F_5^{0.90+}$, with the remaining +0.10 charge distributed among the three BF_3 molecules. One of the BF_3 molecules is doubly coordinated to the B_2F_5 through two of its F atoms, each of which interacts with one of the B atoms in the B_2F_5. The BF_3 thus bridges the two B atoms in the B_2F_5, forming a six-membered ring. These two F−B distances are 2.329 and 2.322 Å, so the coordination is loose. The bond lengths encourage a description of this interaction as van der Waals contact directed by electrostatic attractions between electron-rich, electronegative fluorine and electron-poor boron. The electron density isosurface supports this conclusion with large breaks between these pairs of atoms. The B atom of this first BF_3 has coordinated to it an F atom of a second BF_3; the third BF_3 is similarly coordinated to the B atom of the second. These F−B distances are 2.413 and 2.517 Å, respectively, so these are also weak interactions.

The HF 3-21G(*) result for $B_5F_{14}^+$ involves a different set of fragments. The structure breaks down into $B_2F_5^{0.66+}$, $B_2F_7^{0.24-}$, and $BF_2^{0.58+}$ fragments which are arranged to form a bicyclic, asymmetrically puckered structure with six- and eight-membered rings (Figure 4f). The heptafluorodiborate anion ($B_2F_7^-$) has been observed by X-ray diffraction as a counterion to a Pd complex.[27] The values from our calculations for the bridging B−F−B angle (138.7°) and B−F distances (1.53 and 1.52 Å) in this $B_2F_7^{0.24-}$ compare reasonably well with the X-ray diffraction values [128.1(7)°; 1.50(1) and 1.51(1) Å], though such a comparison is of questionable significance due to the markedly different environments of the two species.

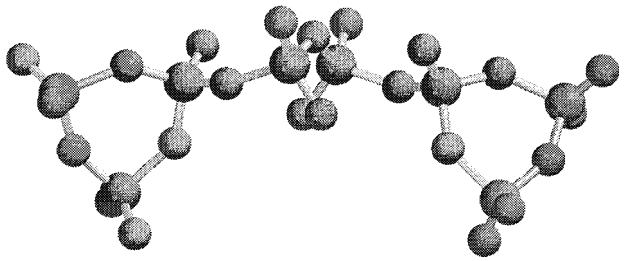

Figure 8. Structure of $B_8F_{23}^+$, optimized at the 3-21G(*) level. The central B_2F_5 is viewed nearly edge on, and the C_2 axis is in the plane of the page. The electron density isosurface is omitted here for clarity. See discussion in text.

5.2. $B_nF_{3n-1}^+$, $n = 6-8$. Optimization of $B_6F_{17}^+$ with the 3-21G(*) basis set yields a structure resembling a BF_3 molecule whose B atom is loosely coordinated to a nonbridging F atom in the six-membered ring of the $B_5F_{14}^+$ described above. The six-membered ring of the $B_5F_{14}^+$ structure appears to contribute sufficiently to the stability of the cluster ion that, though disturbed, it is not broken down by the addition of a BF_3 molecule. $B_7F_{20}^+$ does not optimize to a single, reproducible structure. Rather, the structure obtained from the geometry optimization depends on the initial geometry. The structures obtained can be broken down into parts based on their electron density isosurfaces, and they include some familiar fragments. In one case, the optimized ion breaks down into $BF_3^{0.02-}$, $B_2F_5^{0.68+}$, $B_3F_8^{0.76+}$, and $BF_4^{0.42-}$, while in another case it resembles $BF_3^{0.01+}$, $B_2F_5^{0.62+}$, $B_2F_5^{0.63+}$, and $B_2F_7^{0.27-}$. The second of these two structures is only 3.7 kJ mol^{-1} lower in energy than the first, so it is likely that $B_7F_{20}^+$ is a floppy, highly fluxional cluster ion (see Caveats section).

With $B_8F_{23}^+$, a symmetric structure is once again obtained, as it is predicted at the HF 3-21G(*) level to be a C_2 species (Figure 8). The structure, which combines aspects of the $B_4F_{11}^+$ and $B_5F_{14}^+$ (6-31G*) structures, can be divided into three B_2F_5 units and two BF_4 units. Each B atom of a central distorted B_2F_5 has coordinated to it a BF_4, in a manner reminiscent of the coordination of BF_3 molecules to $B_2F_5^{\delta+}$ seen in $B_4F_{11}^+$. Each of the remaining two B_2F_5 units is coordinated to one of the BF_4 units, forming six-membered rings in a fashion similar to that seen in $B_5F_{14}^+$. The charge distribution again tends in the general direction of the expected closed-shell values for these fragments with a central $B_2F_5^{0.59+}$ coordinated by two $BF_4^{0.41-}$ units and a terminal $B_2F_5^{0.62+}$ on each end. This structure has two important implications. First, the formation of three $B_2F_5^{\delta+}$ units implies that formation of $B_2F_5^+$ is particularly favorable, in agreement with the calculated thermochemistry in Table 3. Second, the idea that the formation of cyclic structures enhances cluster ion stability is supported in that this minimum energy structure has two six-membered rings.

5.3. Caveats. Our first caveat concerns the experimental significance of the calculated structures. A successful geometry optimization converges to a final, minimum-energy, static structure. In contrast, the cluster ions we observe experimentally are formed in a very energetic process, so the final internal energies of the cluster ions must be considered. After electron

TABLE 3: Computationally Derived Thermochemical Values

species	E_{elec}, hartrees	E_{int}, kJ mol^{-1}	$\Delta_f H_{298}$, kJ mol^{-1}	ΔH(BF_3 loss), kJ mol^{-1}
		(a) HF 3-21G(*)		
BF_3	−321.465 844 7	45	−1136.8[a]	
BF_2^+	−222.086 014 4	32	317.0[a]	
$B_2F_5^+$	−543.634 196 8	83	−1029	209
$B_3F_8^+$	−865.146 906 4	135	−2282	116
$B_4F_{11}^+$	−1186.651 687 5	187	−3514	95
$B_5F_{14}^+$	−1508.180 958 4	235	−4813	162
$B_6F_{17}^+$	−1829.655 600 0	288	−5965	15
$B_7F_{20}^+$	−2151.169 185 9	338	−7222	120
$B_8F_{23}^+$	−2472.687 012 7	389	−8488	130
		(b) HF 6-31G*		
BF_3	−323.195 485 4	44	−1136.8[a]	
BF_2^+	−223.310 876 7	33	317.0[a]	
$B_2F_5^+$	−546.556 107 2	83	−944	124
$B_3F_8^+$	−869.770 085 4	133	−2124	43
$B_4F_{11}^+$	−1192.977 793 7	184	−3285	25
$B_5F_{14}^+$	−1516.177 203 5	235	−4425	3

[a] Experimental value from ref 25.

impact ionization, the cluster ions dissipate energy through evaporative loss of BF_3 molecules. This process is complete when a cluster ion retains less internal energy than is required to eject another BF_3 molecule. The cluster ion dissociation energy is thus an upper limit to the energy retained at the completion of evaporative cooling. The values labeled ΔH(BF_3 loss) in Table 3a,b are computational estimates of exactly this dissociation energy. Consideration of the dissociation process allows us to determine whether the magnitudes of these calculated values are reasonable. As a cluster ion loses a neutral molecule, the ion-induced dipole attraction must be overcome. This type of interaction is stronger and operates over greater distances than the induced dipole−induced dipole interactions present in the bulk liquid.[28] Therefore, for a small to moderate size cluster ion this dissociation energy should be larger than the enthalpy of vaporization of the bulk liquid. The maximum possible amount of internal energy in a stable cluster ion is thus at least as large as the bulk enthalpy of vaporization, which is 19.33 kJ mol^{-1} for BF_3 at its normal boiling point of 172 K.[29] At the HF 6-31G* level, all the dissociation energies (except one) are indeed greater than this value for the enthalpy of vaporization. It is therefore possible that many of these ions have internal energies even greater than the equivalent of $\Delta_{vap}H°(BF_3)$. The fact that ΔH(BF_3 loss) for $B_5F_{14}^+$ is only 3 kJ mol^{-1} may mean either that we have not found the global minimum-energy structure for this species or that these ΔH(BF_3 loss) values are systematically underestimated by the calculations.

Cold cluster ions may well take on the calculated structures reported here. As tempting as it is to believe that our true cluster ion structures are represented accurately by these calculated structures, we must conclude that the internal energies of the cluster ions formed in this experiment are probably high enough to result in significant fluxional behavior. Ring opening and closing and shuttling of bridging fluorine atoms between fragments are examples of the types of fluxionality that may be present in these ions. The results discussed above imply that $B_7F_{20}^+$ may be an extreme example of this behavior.

A second caveat must accompany the stated absence of "magic" numbers in our mass spectra. Formation of cyclic structures after ionization is often invoked to explain the presence of magic numbers.[17] Here, our calculations predict the formation of cyclized structures for $B_nF_{3n-1}^+$ with $n = 5-8$. These can be divided into two groups: those with "dangling" BF_3 molecules [$n = 6$, 7 for 3-21G(*), $n = 5$ for 6-31G*] and those without [$n = 5$, 8 for 3-21G(*)]. The computational thermochemistry in Table 3a,b indicates that structures without dangling BF_3 molecules appear to be somewhat more resistant to BF_3 loss than those with them. If the trends in the calculated thermochemical results for the 6-31G* basis set are reflected in the experimentally generated cluster ions, then we would expect to see simple decay in the ion signal as n increases, which is exactly what Figure 2 shows. On the other hand, if the HF 3-21G(*) results were a better representation of the ions, then we might expect to see magic numbers for $n = 5$ and 8.

Our mass spectra offer no evidence of magic numbers. There are at least three possible explanations for this. First, the HF 6-31G* calculations may provide a more accurate picture of the nature of these species. Second, magic numbers proposed to be associated with cyclization or other structural features are typically discussed in terms of formation of covalently bound structures.[17] The structures predicted here include some apparently weaker interactions. These noncovalent (electrostatic) interactions may not be sufficiently strong to exercise any significant influence over the evaporative process that yields the final cluster size distribution. Third, the overall magnitude of our ion signal is small, and the intensity falls off rapidly with cluster size. This raises the possibility that our cluster source simply lacks the intensity to provide a cluster distribution sufficiently broad for the intensity variations caused by structural stability to be visible on top of the simple decay in intensity with cluster size. It is possible, then, that similar experiments with a more intense cluster ion source could reveal intensity maxima for the cyclized structures without dangling BF_3 at $n = 5$ and $n = 8$, though the HF 6-31G* calculations cast some doubt on this prospect.

6. Conclusions and Outlook

Mass spectra resulting from ionization of boron trifluoride clusters have been measured. Ab initio modeling results have informed the interpretation of some cluster ion structures. These structures have directed our speculation as to ion−molecule chemistry which may occur with this ion formation technique. The formation of $B_2F_5^{\delta+}$ appears to be widespread in the $B_nF_{3n-1}^+$ series. The appearance of $BF_4^{\delta-}$ and $B_2F_7^{\delta-}$ in larger cluster ions demonstrates an interesting propensity toward charge separation, probably related to energetically favorable formation of approximately closed-shell fragments.

While the relatively low-level calculations performed here seem adequate for a qualitative understanding of $B_nF_{3n-1}^+$ cluster ion structure, they are probably not quantitatively correct. A potentially fruitful area for further work is therefore higher level calculations on these ions to clarify their structures and energetics and on larger ions in the series to determine growth patterns. Fragmentation experiments, whether surface-induced or collision-induced dissociation or photodissociation, could shed further light on the internal structure of these cluster ions, possibly supporting the presence of moieties such as BF_3, $B_2F_5^+$, BF_4^-, and $B_2F_7^-$ through fragmentation patterns.

No structures resembling the boron subfluorides (B_3F_5, B_8F_{12}, etc.[4−7]) appear to be formed in electron impact of BF_3 clusters. The known boron subfluorides are boron-rich compounds with structures including B−B bonds and only terminal halogens. In contrast, the ions in our mass spectrum have B:F ratios near 1:3, with calculated structures including bridging fluorine atoms and no indication of B−B bonding.

The ions we observe, while different from neutral boron fluorides, share with them the lack of formation of cage-type

compounds.[7,15] However, polyhedral cage structures for boron chlorides and bromides with the formulas B_nCl_n ($n = 4$, $8-12$)[15,30] and B_mBr_m ($m = 7-10$)[15] are known, and mass spectral evidence has been reported for larger B_nCl_n ($n = 13-20$).[31] Experiments are underway to investigate the behavior of BCl_3 and BBr_3 under conditions similar to those described here for BF_3.

A complementary means of studying ion−molecule chemistry in the gas phase, also in use in our laboratory, is to form ions by passing a $1-3$ μs discharge through a mixture of helium and the species of interest and then allow the resulting mixture of ions and neutrals to pass through a flow tube prior to expansion into vacuum for mass analysis. Thermalization and ion−molecule reactions, as well as simple aggregation through three-body collisions, take place in the flow tube. A description of our study of BF_3 by this technique is forthcoming.[32]

Acknowledgment. This work has been supported by the National Science Foundation (CHE-9505444), a William and Flora Hewlett Foundation Award of Research Corporation (CC3484), the Petroleum Research Fund of the American Chemical Society (27155-GB6), and Hendrix College. Brad W. Blackmon, Robert D. English, Brett C. Yates, and Randi Kay Vest provided valuable assistance with the construction and development of the TOFMS and ion sources.

References and Notes

(1) Mo, Y.; Lin, Z. *J. Chem. Phys.* **1996**, *105*, 1046. Samdal, S.; Mastryukov, V. S.; Boggs, J. E. *J. Mol. Struct.* **1996**, *380*, 43. Demachy, I.; Volatron, F. *J. Phys. Chem.* **1994**, *98*, 10728. Zakzhevskii, V. G.; Charkin, O. P. *Chem. Phys. Lett.* **1982**, *90*, 117. Howell, J. M.; Van Wazer, J. R. *J. Am. Chem. Soc.* **1984**, *96*, 7902. Hall, J. H.; Halgren, T. A.; Kleier, D. A.; Lipscomb, W. N. *Inorg. Chem.* **1974**, *13*, 2520. Cowley, A. H.; White, W. D.; Damasco, M. C. *J. Am. Chem. Soc.* **1969**, *91*, 1922. Moore, E. B., Jr. *Theor. Chim. Acta* **1967**, *7*, 144. Kato, H.; Yamaguichi, K.; Yonezawa, T.; Fukui, K. *Bull. Chem. Soc. Jpn.* **1965**, *38*, 2144. Brown, R. D.; Harcourt, R. D. *Aust. J. Chem.* **1963**, *16*, 737. Green, M.; Linnett, J. W. *J. Chem. Soc.* **1956**, 4514.

(2) Danielson, D. D.; Patton, J. V.; Hedberg, K. *J. Am. Chem. Soc.* **1977**, *99*, 6484. Durig, J. R.; Thompson, J. W.; Witt, J. D.; Odom, J. D. *J. Chem. Phys.* **1973**, *58*, 5339. Nimon, L. A.; Seshadri, K. S.; Kalkunte, S.; Taylor, R. C.; White, D. *J. Chem. Phys.* **1970**, *53*, 2416. Finch, A.; Hyams, I.; Steele, D. *Spectrochim. Acta* **1965**, *21*, 1423. Gayles, J. N.; Self, J. *J. Chem. Phys.* **1964**, *40*, 3530.

(3) Korkin, A. A.; Balkova, A.; Bartlett, R. J.; Boyd, R. J.; Schleyer, P. v. R. *J. Phys. Chem.* **1996**, *100*, 5702. Lin, C.-S.; Li, J.; Liu, C.-W. *Chin. J. Chem.* **1994**, *12*, 305. Swanton, D. J.; Ahlrichs, R. *Theor. Chim. Acta*, **1989**, *75*, 163. Kleier, D. A.; Bicerano, J.; Lipscomb, W. N. *Inorg. Chem.* **1980**, *19*, 216. Hall, J. H.; Lipscomb, W. N. *Inorg. Chem.* **1974**, *13*, 710. Massey, A. G.; Urch, D. S. *J. Chem. Soc.* **1965**, 6180.

(4) Timms, P. L. *J. Am. Chem. Soc.* **1967**, *89*, 1629.

(5) Kirk, R. W.; Smith, D. L.; Airey, W.; Timms, P. L. *J. Chem. Soc., Dalton Trans.* **1972**, 1392.

(6) Hartman, J. S.; Timms, P. L. *J. Chem. Soc., Dalton, Trans.* **1975**, 1373.

(7) Timms, P. L. *Acc. Chem. Res.* **1973**, *6*, 118.

(8) Gandia, J. J.; Gutiérrez, M. T.; Cárabe, J. *Thin Solid Films* **1993**, *223*, 161. Kakinuma, H.; Mohri, M.; Tsuruoka, T. *J. Appl. Phys.* **1993**, *74*, 4614.

(9) Husein, I. F.; Zhou, Y.; Qin, S.; Chan, C. *Surf. Eng.* **1997**, *13*, 56.

(10) Shao, J.; Round, M.; Qin, S.; Chan, C. *J. Vac. Sci. Technol. A* **1995**, *13*, 332. Jones, E. C.; En, W.; Ogawa, S.; Fraser, D. B.; Cheung, N. W. *J. Vac. Sci. Technol. B* **1994**, *12*, 956.

(11) Farber, M.; Srivastava, R. D. *J. Chem. Phys.* **1984**, *81*, 241.

(12) Batten, C. F.; Taylor, J. A.; Tsai, B. P.; Meisels, G. G. *J. Chem. Phys.* **1978**, *69*, 2547. Berger, H.-O.; Kroner, J.; Nöth, H. *Chem. Ber.* **1976**, *109*, 2266. King, G. H.; Krishamurthy, S. S.; Lappert, M. F.; Pedley, J. B. *Faraday Discuss. Chem. Soc.* **1972**, *54*, 70. Bassett, P. J.; Lloyd, D. R. *J. Chem. Soc. A* **1971**, 1551. Marriott, J.; Craggs, J. D. *J. Electron. Control* **1957**, *3*, 194. Law, R. W.; Margrave, J. L. *J. Chem. Phys.* **1956**, *25*, 1086.

(13) Dibeler, V. H.; Liston, S. K. *Inorg. Chem.* **1968**, *7*, 1742.

(14) Lynaugh, N.; Lloyd, D. R.; Guest, M. F.; Hall, M. B. Hillier, I. H. *J. Chem. Soc., Faraday Trans. 2* **1972**, *68*, 2192.

(15) Massey, A. G. *Adv. Inorg. Chem. Radiochem.* **1983**, *26*, 1 and references therein.

(16) See, for example: Vaidyanathan, G.; Garvey, J. F. *J. Phys. Chem.* **1994**, *98*, 2248. Vaidyanathan, G.; Lytkey, M. Y. M.; Stry, J. S.; DeLeon, R. L.; Garvey, J. F. *J. Phys. Chem.* **1994**, *98*, 7475. Garvey, J. F.; Peifer, W. R.; Coolbaugh, M. T. *Acc. Chem. Res.* **1991**, *24*, 48. Coolbaugh, M. T.; Garvey, J. F. *Chem. Soc. Rev.* **1992**, 163. El-Shall, M. S.; Marks, C.; Sieck, L. W.; Meot-Ner, M. *J. Phys. Chem.* **1992**, *96*, 2045. El-Shall, M. S.; Schriver, K. E. *J. Chem. Phys.* **1991**, *95*, 3001.

(17) See, for example: Coolbaugh, M. T.; Whitney, S. G.; Vaidyanathan, G.; Garvey, J. F. *J. Phys. Chem.* **1992**, *96*, 9139. Whitney, S. G.; Coolbaugh, M. T.; Vaidyanathan, G.; Garvey, J. F. *J. Phys. Chem.* **1991**, *95*, 9625. Coolbaugh, M. T.; Vaidyanathan, G.; Peifer, W. R.; Garvey, J. F. *J. Phys. Chem.* **1991**, *95*, 8337. El-Shall, M. S.; Marks, C. *J. Phys. Chem.* **1991**, *95*, 4932.

(18) See, for example: Zhong, Q.; Poth, L.; Shi, Z.; Ford, J. V.; Castleman, A. W., Jr. *J. Phys. Chem. B* **1997**, *101*, 4203. El-Shall, M. S.; Yu, Z. *J. Am. Chem. Soc.* **1996**, *118*, 13058. Grover, J. R.; Cheng, B.-M.; Herron, W. J.; Coolbaugh, M. T.; Peifer, W. R.; Garvey, J. F. *J. Phys. Chem.* **1994**, *98*, 7479. Young, M. A. *J. Phys. Chem.* **1994**, *98*, 7790. Li, S.; Bernstein, E. R. *J. Chem. Phys.* **1992**, *97*, 7383. Jouvet, C.; Lardeux-Dedonder, C.; Richard-Viard, M.; Solgadi, D.; Tramer, A. *J. Phys. Chem.* **1990**, *94*, 5041.

(19) Echt, O. *Elemental and Molecular Clusters*; Benedek, G., Martin, T. P., Pacchioni, G., Eds.; Springer-Verlag: Berlin, 1988; p 263.

(20) Wiley, W. C.; McLaren, I. H. *Rev. Sci. Instrum.* **1955**, *26*, 1150.

(21) Sattler, K.; Muhlbach, J.; Echt, O.; Pfau, P.; Recknagel, E. *Phys. Rev. Lett.* **1981**, *47*, 160.

(22) Castleman, A. W., Jr.; Märk, T. D. *Gaseous Ion Chemistry and Mass Spectrometry*; Futrell, J. H., Ed.; John Wiley & Sons: New York, 1986; p 270.

(23) Jortner, J.; Scharf, D.; Landman, U. *Elemental and Molecular Clusters*; Benedek, G., Martin, T. P., Pacchioni, G., Eds.; Springer-Verlag: Berlin, 1988; p 148.

(24) Lias, S. G.; Bartmess, J. E.; Liebman, J. F.; Holmes, J. L.; Levin, R. D.; Mallard, W. G. *J. Phys. Chem. Ref. Data* **1988**, *17* (Suppl. No. 1).

(25) Lias, S. G.; Liebman, J. F.; Levin, R. D.; Kafafi, S. A. *NIST Standard Reference Database 19A: Positive Ion Energetics*, version 2.0; National Institute of Standards and Technology: Gaithersburg, MD, 1993.

(26) Frum, C. I.; Engleman, R., Jr.; Bernath, P. F. *J. Chem. Phys.* **1991**, *95*, 1435. Snelson, A. *J. Phys. Chem.* **1966**, *70*, 3208. Büchler, A.; Stauffer, J. L.; Klemperer, W. *J. Chem. Phys.* **1964**, *86*, 4544.

(27) Braunstein, P.; Douce, L.; Fischer, J.; Craig, N. C.; Goetz-Grandmont, G.; Matt, D. *Inorg. Chim. Acta* **1992**, *194*, 151.

(28) Levine, R. D.; Bernstein, R. B. *Molecular Reaction Dynamics and Chemical Reactivity*; Oxford University Press: New York, 1987; pp 102−103.

(29) *CRC Handbook of Chemistry and Physics*, 75th ed.; Lide, D. R., Ed.; CRC Press: Boca Raton, FL, 1994; p 6−110.

(30) Davan, T.; Morrison, J. A. *Inorg. Chem.* **1986**, *25*, 2366.

(31) Saulys, D. A.; Kutz, N. A.; Morrison, J. A. *Inorg. Chem.* **1983**, *22*, 1821.

(32) Hales, D. A.; Barker, M. P.; Haile, P. A.; Hunt, H. L. Manuscript in preparation.